Flux distribution analysis of central metabolic pathways in *Desulfovibrio vulgaris* Hildenborough using GC-MS and FT-ICR mass spectrometry.

Yinjie Tang†[1,2], Francesco Pingitore†[1,2], Aindrila Mukhopadhyay†[1,2], Richard Phan[1,3], Terry C. Hazen[1,3] Jay D. Keasling[1,2,4*].

Virtual Institute of Microbial Stress and Survival[1], Physical Biosciences Division, Lawrence Berkeley National Laboratory, Berkeley, USA[2], Earth Sciences Division, Lawrence Berkeley National Laboratory, Berkeley, USA[3], Departments of Chemical Engineering and Bioengineering, University of California, Berkeley, USA[4]

*Corresponding author

Prof. Jay D. Keasling

Berkeley Center for Synthetic Biology,

717 Potter Street, Berkeley, CA, 94720 USA

Email: keasling@berkeley.edu

Phone: 510-495-2620, Fax: 510-495-2630

†: These authors contributed equally in this study

Abstract

Flux distribution in central metabolic pathways of *Desulfovibrio vulgaris* Hildenborough was examined using ^{13}C tracer experiments. Consistent with the current genome annotation and independent evidence from enzyme activity assays, the isotopomer results from both GC-MS and Fourier Transform-Ion Cyclotron Resonance mass spectrometry (FT-ICR MS) indicate the lack of oxidatively functional TCA cycle and an incomplete pentose phosphate pathway. Results from this study suggest that fluxes through both above pathways are limited to biosynthesis. The data also indicate that the lactate→acetate pathway is the main carbon flow (>80% lactate is converted to acetate) and energy generation route (>90% NAD(P)H and ATP production), and that acetyl-CoA can be directly oxidized via a reversible pathway not involving reactions of the TCA cycle. Acetyl-CoA oxidation also produces NADH and ATP as well as 5,10-methyl-THF and CO. Although the genome annotation implicates a ferredoxin-dependent oxoglutarate synthase, isotopic evidence does not support flux through this reaction in either the oxidative or reductive mode; therefore, the TCA cycle is incomplete. FT-ICR MS was used to locate the labeled carbon distribution in aspartate and glutamate and confirmed the presence of an atypical enzyme for citrate formation suggested in previous reports (citrate produced is the isotopic antipode of the citrate synthesized by the (S)-citrate synthase). These findings enable a better understanding of the relation between genome annotation and actual metabolic pathways in *D. vulgaris*, and also demonstrate FT-ICR MS as a powerful tool for isotopomer analysis, overcoming problems in both GC-MS and NMR spectroscopy.

Key words: genome annotation, TCA cycle, pentose phosphate pathway, acetyl-CoA, atypical citrate synthase, FT-ICR MS

Introduction

Sulfate reducing bacteria (SRB) such as *Desulfovibrio vulgaris* Hildenborough are ubiquitous in nature and play an important role in global sulfur cycling and the mineralization of organic matter (21, 39, 40). The uncontrolled growth of *D. vulgaris* contributes to bio-corrosion of oil and gas pipelines and the souring of production wells (18, 37, 54). Conversely, the ability of *D. vulgaris* to reduce heavy metals and radionuclides to more insoluble forms provides a unique microbe-oriented solution for bioremediation (25, 27, 28). In addition to its environmental importance, *D. vulgaris* has unique energy metabolism that has the potential to be used for hydrogen or methane production in either pure or mixed cultures (7, 13, 38, 50).

The availability of an annotated genome sequence for *D. vulgaris* (25) makes it an ideal organism for investigation of SRB physiology, and several functional genomics studies have described the transcriptome and proteome of this organism (10, 24, 35). Information from these analyses is critical for validating genome annotation and predictions for operons and regulons. Moreover, *D. vulgaris* metabolism has been studied for several decades, but the recently published annotated genomic sequence of *D. vulgaris* contained some unresolved predictions related to key pathways (25). 1) Although the TCA cycle lacks a typical 2-oxoglutarate dehydrogenase, a ferredoxin-dependent 2-oxoglutarate synthase (9) homolog (EC 1.2.7.3, 2-oxoglutarate ←→ succinyl-CoA) has been annotated for this step. 2) While the annotation predicts pathways for respiration using sulfate and other terminal electron acceptors, whether the TCA cycle functions oxidatively (via the ferredoxin-dependent 2-oxoglutarate synthase) or only reductively remains to be determined. 3) Although citrate synthases have been reported in other δ-proteobacteria (6), neither *D. vulgaris* nor the closely-related *D. desulfuricans* G20 contains a citrate synthase homolog in the annotated genome. However, these organisms are not

auxotrophic for amino acids typically derived from citrate, and previous experiments have suggested the presence of an atypical enzyme that enables the production of citrate in *Desulfovibrio* spp. (19, 20, 34).

Metabolic flux analysis is an ideal method to link genome annotation to cellular phenotypes (14), and isotopomer analysis is the *in vivo* method of choice to examine cellular metabolic pathways (45). Analysis of isotopomer distributions in metabolites (often amino acids) requires advanced techniques such as nuclear magnetic resonance (NMR) spectroscopy or mass spectrometry. Although NMR spectroscopy can be used to determine the location of the ^{13}C label in individual isotopomers, not all isotopomers can be detected using this technique, since carbon atoms separated by more than one bond do not influence each other's resonance sufficiently (43). Further, labeled carbon sources that result in metabolites with the isotopic label solely on a carboxyl carbon are difficult to address using common ^{13}C NMR techniques. Additionally, though non-destructive, the sensitivity of an NMR-based technique is low, necessitating a large amount of costly labeled culture. Among mass spectroscopic techniques, gas chromatography coupled to mass spectrometry detection (GC-MS) is typically the technology of choice since it requires much less sample, and isotopomer analysis software tools enable quick identification of the isotopomer pattern. By examining different mass fragments, one can determine certain labeling positions, such as labeling on an α-carboxyl group. But GC-MS alone cannot locate all labeled positions in amino acids or organic acids.

In contrast to GC-MS and NMR spectroscopy, Fourier Transform-Ion Cyclotron Resonance mass spectrometry (FT-ICR MS) provides, with direct injection (i.e., without chromatographic separation of sample), an accurate mass determination of many of the metabolites in complex mixtures (8, 32). Furthermore, Electrospray Ionization (ESI) is

amenable to polar compounds without the need for derivatization, eliminating the need to correct for isotope distributions in the derivatizing agent. An additional advantage of FT-ICR MS is its ability to detect metabolites in the low nanomolar range. As a trapping technique, FT-ICR MS performs multiple stages of mass spectrometric events (MS^n) utilizing Collision Induced Dissociation (CID). Detection of mass/charge ratios as low as 30 can be achieved in the ICR cell (32), and mass spectrometric fragmentation patterns of amino acids are very well understood (4, 22, 23, 29, 52). This study outlines the utilization of ESI FT-ICR MS to localize the position of ^{13}C atoms in metabolites of interest and represents an important complimentary technique to GC-MS for pathway annotation and metabolic flux analysis in *D. vulgaris*.

Materials and Methods

Bacterial growth and maintenance. *Desulfovibrio vulgaris* Hildenborough was obtained from the American Type Culture Collection (ATCC 29579, Manassas, VA). All experiments used defined lactate sulfate medium, LS4D (35), with the modification that titanium citrate was not used. The inoculum for all experiments was started from fresh frozen stock (unlabeled culture). Isotopic labeling experiments were run in triplicate using LS4D medium containing 99% [1-^{13}C]-L-lactate (Cambridge Isotope, USA) with a 1:10 inoculation volume. The culture in the exponential phase (OD_{600}=0.4) was used as inoculum for sub-culture. To remove the effects of unlabeled lactate and glycerol from the initial stock culture, two sequential 10% subcultures into labeled medium were performed to obtain the final culture. All incubations were performed at 30°C in an anaerobic chamber (Coy Laboratory Products Inc, Grass Lake, MI, USA) with an atmosphere of 5% CO_2, 5% H_2, and 90% N_2.

Analysis of extracelluar metabolites and biomass composition. Cell growth was monitored by measuring both optical density at a wavelength of 600 nm (OD_{600}) and total protein

concentration using the Bradford Protein Assay (BioRad Laboratories, Hercules, CA, Cat. no. 500-0006). The concentrations of pyruvate, succinate, lactate and acetate in the medium were measured using enzymatic kits (r-Biopharm, Darmstadt, German). To measure biomass weight, 50 ml of cells were centrifuged at 4800 × g and 4°C for 20 min, the cell pellet was dried in a lyophilizer (Labconco, Cat#7420020, Kansas City, MI) for 24 hours, and the dried weight was determined by gravimetry. Fatty acids were quantified in the dried biomass using previously described methods (48), performed by Microbial ID (Newark, Delaware). Amino acids were also quantified in the dried biomass using the Beckman 6300 amino acid analyzer (Beckman Coulter, California), performed by Molecular Structure Facility at the University of California, Davis. Sulfate concentration was determined by reaction with barium chloride and absorbance measurement at a wavelength of 450 nm (13). All measurement methods for biomass constituents (carbohydrates, RNA, and DNA) were conducted using previous reported protocols (15, 31). Briefly, carbohydrate was quantified using the phenol reaction, RNA was assayed using the orcinol reaction method, and DNA was measured using a colorimetric procedure that involves the reaction of DNA with diphenylamine in a mixture of perchloric acid. Glucose, pure *E. coli* RNA (Ambion #7940, Austin, TX), and deoxyribose were used as standards for the carbohydrate, RNA, and DNA measurements, respectively.

GC-MS procedure. In order to measure amino acid labeling patterns in cellular protein, the biomass was harvested by centrifuging at 10,000 × g and 4°C for 20 minutes and lysed via sonication in deionized water. Sonication was conducted using a micro-tip for 3 minutes with pulses of 3 seconds on and 1 second off. The protein from the resulting lysate was precipitated using trichloroacetic acid and then hydrolyzed in 6 M HCl at 100°C for 24 hours. In the resulting amino acid mixture, cysteine and tryptophan were lost due to oxidation, and glutamine and

asparagine were deaminated. GC-MS samples were prepared in 100 µl of tetrahydrofuran (THF) and 100 µl of N-(tert-butyldimethylsilyl)-N-methyl-trifluoroacetamide (Sigma-Aldrich, St. Louis, USA). All samples were derivatized in a water bath at 65-80°C for 1 hour, producing tert-butyldimethlysilyl (TBDMS) derivatives. One µl of the derivatized sample was injected into GC-MS: a gas chromatograph (Agilent HP6890, Wilmington, DE) equipped with a DB5-MS column (J&W Scientific, Folsom CA) and analyzed using a mass spectrometer (Agilent 5973, Wilmington, DE). The GC operation conditions were: the GC column was held at 150°C for 2 minutes, heated at 3°C per minute to 280°C, heated at 20°C per minute to 300°C, and held for 5 minutes at that temperature.

To prepare GC-MS samples using bis(trimethylsilyl)trifluoroacetamide (BSTFA) as the derivatization reagent (measure, lactate, pyruvate and succinate labeling pattern), 0.5 ml of supernatant was frozen in liquid nitrogen and then lyophilized overnight. The dried samples were pre-derivatized with a solution (0.3 ml) of 2% hydroxylamine hydrochloride (Fluka, Milwaukee, WI, USA) in pyridine (Sigma-Aldrich, St. Louis, USA) overnight at room temperature. Following this, each sample was derivatized at room temperature for 25 min using 0.5 ml BSTFA (Sigma-Aldrich, USA) before measurement by GC-MS. This derivatization added trimethylsilyl (TMS) groups to carboxyls and converted oxoacids (e.g., pyruvate) to oximes for greater MS suitability. Decane (Aldrich Chemical, USA) was used as an internal standard. One µl of the derivatized sample was injected into GC-MS. The column was held at 60°C for one minute after injection, and then heated at 20°C/min to 130°C, 4°C/min to 150°C, and finally 40°C/min to 260°C, where it was held for 3 min. Helium carrier gas was used at a column flow rate of 1.2 ml/min with a 1:20 split ratio at injection.

FT-ICR spectrometry

For ESI FT-ICR MS analysis, the supernatant or the dried hydrolyzed mixture sample was prepared in 1 ml of MeOH/H_2O (1/1) mixture plus 1% formic acid. The resulting solution was amenable to ionization with an electrospray source. The analysis was performed on an Apex III FT-ICR MS (Bruker Daltonics, Billerica, MA, USA) equipped with 9.4 Tesla actively shielded magnet. Ions were generated using the Apollo I ESI source in positive ion mode at a flow rate 120 µl/min, nebulizing gas pressure of 40 PSI, dry gas temperature of 175°C with source voltages of -4.4 kV on the atmospheric side of the capillary, -4.0 kV on the end cap shield, and -2.0 kV on the cylinder shield. After this stage, ions were accumulated for 2 sec in an external hexapole ion guide and transferred to the cell with a background pressure of ~$5x10^{-11}$ mbar for detection. The operating software was XMASS version 6.0 (Bruker Daltonics, USA). Each spectrum was composed of 32 scans. Multiple stage mass spectrometry experiments were carried out by isolating the ions of interest and activating them by SORI-CID in the ICR cell (29).

Annotated pathway map and algorithm for flux calculation. The key biochemical pathways included in the *D. vulgaris* model were glycolysis, the TCA cycle, and the pentose phosphate (PP) pathway (1) (Figure 1). Each reaction and its corresponding gene are listed in (Supplementary Table S-1). Extracellular concentrations of pyruvate, acetate and succinate were measured directly using enzymatic methods. The remaining unknown fluxes were determined based on network stoichiometries and isotopomer data (45). The fluxes through the pool of amino acids, carbohydrate, and RNA/DNA are dependent on the biomass production and the measured average biomass composition (Supplementary Table S-2) (45).

The reversible reactions are characterized by their net flux, v_i, and their exchange flux, v_i^{exch}. The net flux is defined as the difference between forward and backward fluxes, ($v_i^{\rightarrow}$- $v_i^{\leftarrow}$). The exchange flux, v_i^{exch}, is the smaller of the forward and backward fluxes, min($v_i^{\rightarrow}$, $v_i^{\leftarrow}$), and is used to calculate the exchange coefficient, $exch_i$, according to (57)

$$v_i^{exch} = \frac{exch_i}{1 - exch_i} \tag{1}$$

Exchange coefficient values for key reactions were searched globally in the range [0 1]. All reactions could be potentially reversible and make the system highly underdetermined (45). To simplify model calculation, reactions in PP pathway, were considered to be unidirectional because they are used only for biosynthesis and the reversibility had the least significant impact on the isotopomer distribution. Additionally, the isotopomer data was not sensitive to the reversibility of some reactions (e.g., PYR→MAL and PYR→OAA) and thus they were also not considered to be reversible (2, 58).

By using the concept of atomic mapping matrices (AMM) (Supplementary Table S-3) (42, 43), the steady-state isotopomer distributions in the intracellular metabolite pools were obtained (MATLAB 6.0, The Mathworks, USA); these isotopomer distributions were used to simulate MS data (m/z=M0, M1, M2…). The optimal solution was found based on an objective function defined as:

$$\varepsilon(v_n) = \sum_{i=1}^{a} \left(\frac{M_{i,m} - M_{i,c}(v_n)}{\delta_i} \right)^2 \tag{2}$$

where v_n is the unknown fluxes to be optimized in the program, $M_{i,m}$ are the measured MS data, and $M_{i,c}$ are the corresponding model-simulated MS data. The flux estimations can be calculated using the simulated annealing concept for all unknown fluxes to achieve a minimal ε (2). In order to verify whether the TCA cycle functions oxidatively or is incomplete, two model

programs were constructed, one for a complete TCA cycle and one for an incomplete TCA cycle. By comparing the simulation results from two independent programs, only the model with the correct assumption for the TCA cycle resulted in final predictions consistent with all the measurement data and thus clarified the actual operation of the TCA cycle reactions in *D. vulgaris.* The MATLAB programs for calculation of flux and exchange coefficients can be obtained at http://vimss.lbl.gov/DvHFlux//.

Results

***D. vulgaris* growth kinetics in LS4D medium.** *D. vulgaris* was grown in LS4D medium with [1-^{13}C]-L-lactate as the sole carbon and energy source; acetate was the main product (Table 1). For biomass growth, lactate and sulfate consumption, and acetate secretion see supplementary Figure S-1 and S-2. When grown in medium containing isotopically labeled lactate, the *D. vulgaris* doubling time was 8~9 hours, with a mid-log phase density of ~4×10^8 cells/ml (OD_{600} 0.35), and corresponding biomass weight was 132±22 mg/L. The final cell density was ~ 10^9 cells/ml (OD_{600} 0.7) after 45 hours. The elemental composition of *D. vulgaris* was reported to be $CH_{1.64}N_{0.23}O_{0.33}S_{0.01}P_{0.014}$ (51). The weight fraction of biomass components was 0.39±0.04 protein, 0.l4±0.03 RNA/DNA, 0.19±0.05 carbohydrate, 0.16±0.02 ash, 0.05±0.01 fatty acids, and 0.07±0.03 other. Due to precipitation of metals by *D. vulgaris* during the experimental growth period, total protein concentration in the culture rather than OD_{600}, more accurately reflected the total biomass (Supplemental Figure S-1). The growth kinetics could be described using a typical Monod model, and the fitted model parameters (using nonlinear least square fitting, supplementary data, Figure S-1 and S-2) in this experiment were compared with reported values (Table 1):

$$\mu = \frac{\mu_{\max} C_L}{K_S + C_L} \quad (3)$$

where μ_{max} is the maximum specific growth rate, C_L is the lactate concentration, and K_S is the Monod saturation constant for lactate (5).

Growth kinetics (Table 1) showed that the minimal doubling time was 8.2 hrs, the fitted specific growth rate was approximately 0.10 hr^{-1}, and the Monod constant was 27 mM. An overall gross biomass yield for lactate was 6.1 g/mol lactate. Complete oxidization of one mole lactate requires consumption of 12 mole e^-, i.e., 1.5 mole sulfate/mole lactate, but the yield coefficient of sulfate/lactate in this study was only 0.4. Trace amounts of pyruvate and succinate were detected, but neither formate nor ethanol accumulated in the medium. Compared to results from *D. vulgaris* growth experiments in lactate medium with amino acid supplements (51), the minimal medium in this study resulted in lower acetate production (only 84% of the lactate was partially oxidized to acetate rather than the 97% found in amino acid-supplemented medium). It was assumed that the lactate not converted to acetate was assimilated into biomass or was completely oxidized.

Mass spectrometry techniques for profiling isotopomer distribution pattern. In order to investigate anaerobic pathways and fluxes under steady-state growth conditions, cells were grown in batch cultures and harvested in the exponential growth phase from batch cultures (a quasi steady state); additionally, this approach is less expensive than continuous culture methods (16, 41, 44). Two types of positively charged species were clearly observed by GC-MS in this study: unfragmented molecules [M-57] and fragmented species that had lost one carboxyl group [M-159] (Supplementary Figure S-3). For amino acids containing two carboxylic groups, namely aspartic acid and glutamic acid, the loss of the α-carboxyl is preferred due to the α-cleavage initiated by the radical site on the nitrogen atom of the amino group (33). The two fragmented

molecules [M-57 and M-159] were used to determine if the α-carboxyl group was labeled. The natural abundance of heavy isotopes common in organic molecules as well as the derivatization agents, including ^{13}C (1.13%), ^{18}O (0.20%), ^{29}Si (4.70%), and ^{30}Si (3.09%), complicate the resulting mass isotopomer spectrum. The effects of these isotopes on mass fragment distributions of key metabolites were corrected using published algorithms before the data were used to calculate the lactate-derived ^{13}C label distribution (26, 55). The correction program (Steve Van Dien, Genomatica Company, San Diego, USA) can be found at http://vimss.lbl.gov/DvHFlux/. Table 2 lists isotopomer distributions for nine targeted amino acids as well as lactate and succinate. Complete information for the isotopomer distribution of each amino acid and the standard errors from GC-MS measurement is provided in supplementary materials (Table S-4).

Profiling a complex mixture of metabolites with MS typically requires the use of a chromatographic separation prior to detection. With the precise accurate mass determination provided by FT-ICR MS, all the amino acids, corresponding isotopomers and other components of the sample could be identified without separation. With external calibration the FT-ICR MS gave, in some cases, mass errors < 1 ppm (e.g. ^{13}C-alanine vs. ^{13}C-proline) and an average error < 2 ppm. Unlike raw data from GC-MS, which is heavily skewed by the natural abundance from the derivatization agent, the isotopomer abundances of the key metabolites from FT-ICR MS can be used directly without correction. Furthermore, FT-ICR MS data matched results obtained by GC-MS for most of amino acids (supplemental materials Table S-4), which indicates that FT-ICR MS is another very valuable technique for isotopomer analysis.

The experimental isotopomer distributions (Table 2 and supplemental materials Table S-4) were used to check whether detected labeling patterns were consistent with the pathways deduced from the annotated genome. Similarity of isotopomer patterns in some amino acids

confirmed that these amino acids were derived from the same precursor. Examples are threonine and aspartate from oxaloacetate, tyrosine and phenylalanine from phosphoenolpyruvate and erythrose-4-phosphate. Since this is redundant isotopomer information (17), only one from each precursor was used in the model calculation (Table 2). For some key amino acids including glycine, alanine, serine and aspartate, the isotopomer distribution after the loss of the first carboxyl group showed that the ^{13}C label was localized to the carboxyl group, indicating that the carbon backbone of these amino acids is from pyruvate, which is also mainly labeled at the carboxyl group.

Confirmation of atypical citrate synthase pathway via FT-ICR MS. The presence of an atypical citrate synthase has been shown in several anaerobic bacteria, including *Desulfovibrio spp.* and *Clostridium kluyveri*, and was named (R)-citrate synthase because it produces citrate with a stereochemistry opposite to that normally observed (19, 20). This atypical pathway (Figure 2) was determined by Gottschalk *et al* using *in vitro* or *in vivo* radioactive ^{14}C tracer experiments, and required enzymatic cleavage and release of the glutamate carboxyl groups as $^{14}CO_2$ to pinpoint the location of the labeled carbon in glutamate.

Here we describe a swift and precise method to confirm the atypical pathway via an *in vivo* non-radioactive ^{13}C tracer experiment. This method relied solely on FT-ICR MS, because GC-MS can only identify the labeled position on C1-carboxyl group, and because it is difficult to use 1D or 2D ^{13}C-NMR spectroscopy to ascertain if one or both of the second or third position carbons in the two amino acids are labeled (47). The structures of product ions generated by fragmentation of glutamic and aspartic acid during FT-ICR MS are well documented (22, 23). For this reason, any shift in the product ions allows an unambiguous assignment of the position of the ^{13}C in the amino acid backbone. The fragmentation of glutamic acid (Figure 3a) showed a

combined loss of H_2O and CO (with nominal mass equal to m/z 103), involving the C1-carboxyl group, in line with the known instability of α-aminoacylium ions (4). Furthermore, the appearance of the peak corresponding to m/z 85 (Figure 3b) involves, in some sequence, the overall loss of two H_2O and one CO from the C1 position. This result accurately matches the fragmentation that gives rise to the m/z 103 ion. Although these results rule out the presence of the ^{13}C in the C1 position, they still do not pinpoint the labeled atom on the amino acid backbone and necessitate another fragmentation event, i.e. an MS^3 experiment. The product ion at m/z 85 has a high abundance and consequently is a good candidate for fragmentation to obtain the diagnostic product ions. In fact, the fragmentation of m/z 85 shows a ^{13}CO loss (Figure 3b), unequivocally identifying the position of the labeled carbon at the C5 position. All mass errors were below 1 ppm, and in some cases even below 0.1 ppm, enabling the isolation and fragmentation of the ions of interest with accurate mass measurements. The FT-ICR MS method was also used for localization of ^{13}C incorporated into aspartic acid (Supplementary materials Table S-5). In aspartic acid, the result indicates that the labeled C always localized to either one or both of the carboxylic groups. The transitions of the carbons in the TCA cycle metabolites of *D. vulgaris* are illustrated in Figure 2.

Determination of the flux distribution using the isotopomer model and reported enzyme activities. Isotopomer analysis is a useful approach for determining the fluxes through branching pathways that converge later (such as glycolysis and the PP pathway), or the fluxes through metabolic cycles (such as the TCA cycle) (Figure 1). The lactate flux (taken to be 100) branched into three pathways at pyruvate. The major flow was into the TCA cycle; the second flow into gluconeogenesis and the PP pathway; and the third flow towards biomass production (e.g., synthesis of alanine, valine, etc.). Approximately 84% of the lactate was partially oxidized to

acetate via acetyl-CoA and this route was a main source for ATP production for *D. vulgaris*. About 5% of lactate was oxidized completely via a carbon monoxide dehydrogenase pathway (49, 53).

The flux results indicated the absence of flux through 2-oxoglutarate ←→ succinate; that is, the TCA cycle is branched and ends with glutamate and succinate. The flux through the glyoxylate shunt also converged to zero using the model optimization, consistent with the absence of isocitrate lyase in this pathway (30). In a branched TCA cycle, four reactions (pyruvate → malate, pyruvate → oxaloacetate, phospho*enol*pyruvate ←→ oxaloacetate, and malate ←→ oxaloacetate) are not distinguishable by isotopomer analysis, because two pairs of molecules (pyruvate and phospho*enol*pyruvate, and malate and oxaloacetate) have the same carbon backbones. In order to have a unique solution, the pathway was further simplified using the assumption that there were no fluxes through oxaloacetate ←→ malate and phospho*enol*pyruvate ←→ oxaloacetate, because of a lack of key enzymes for the two reactions: PEP carboxylase is not found in the annotated genome, while malate dehydrogenase activity was found to be absent in *D. vulgaris* (30).

The flux distribution results and the reversibility of major fluxes are presented in Figure 1. The predicted labeling pattern of all metabolites, based on calculated fluxes and exchange coefficients, reasonably matches the measured data (Figure 1, Table 2). Deviations between the modeled and measured isotopomer data could arise from several sources: 1) differences in biological replicates and in the measurements of the biosynthetic fluxes based on the biomass composition; 2) the noise affecting accuracy of MS data for low abundance ions; and 3) the effect of overlay of certain mass peaks; for example, in GC-MS, the (f302)+ peak may reduce the measurement accuracy for leucine (M-57)+ peak, while isoleucine and leucine peaks are

indistinguishable by FT-ICR MS. 4) Possible reactions affecting pathway of some amino acids, for example, the precursor of leucine (2-oxoisocaproate) may exchange its carboxyl group with $^{12}CO_2$ or $^{13}CO_2$ generated by the decarboxylation of labeled metabolites (36).

Discussion

Though initial genome annotation provided a preliminary overview for *D. vulgaris* metabolism, mis-annotation is possible due to a lack of homology between genes/enzymes in the target organism and those in related or unrelated organisms. For instance, the published annotated genome sequence indicates that several amino acid synthesis pathways (e.g., lysine, methionine, histidine and alanine) are incomplete (1). However, *D. vulgaris* is able to grow in minimal medium, and therefore must contain complete amino acid synthesis pathways. The reverse is also true, i.e. having an annotated gene or genes for a metabolic pathway may not guarantee the presence of the pathway. For example, although the annotated genome sequence for *D. vulgaris* has genes encoding all of the enzymes in glycolysis, our previous experiments showed that *D. vulgaris* is not able to grow on glucose or fructose (unpublished data). Therefore accurate genome annotation requires further curation or biochemical confirmation via enzymatic or tracer experiments.

Pyruvate ←→ acetyl-CoA is a key reaction in *D. vulgaris* metabolism. The genome annotation indicates that *D. vulgaris* has no pyruvate dehydrogenase, but *D. vulgaris* can convert pyruvate to acetyl-CoA and CO_2 via an oxidoreductase. *D. vulgaris* also contains a pyruvate formate lyase enzyme to convert pyruvate to acetyl-CoA and formate without generating NADH; then formate can be further oxidized by formate dehydrogenase to CO_2, generating NADH. Although ^{13}C-L-lactate was the sole carbon and energy source in the growth medium, much less pyruvate (81%) was labeled (precursor to alanine). This may be explained by the highly

reversible reaction (pyruvate ←→ acetyl-CoA + CO_2 or formate) (*exch* = 0.99, equation 1) that exchanges unlabeled carbon from dissolved CO_2 in the medium. Such high reversibility is not surprising because this reaction can be catalyzed by several enzymes (25), including pyruvate synthase, pyruvate formate-lyase, pyruvate:ferredoxin oxidoreductase and oxo-organic acid oxidoreductase present in *D. vulgaris*. These enzymes may also be able to convert acetate to pyruvate if a significant amount of hydrogen and CO_2 were present in the atmosphere of the anaerobic hood (5% H_2 and 5% CO_2) (3). Furthermore, this bacterium contains dihydrolipoyl dehydrogenase (EC 1.8.1.4), which acts on a sulfur group of donors and uses NAD^+ or $NADP^+$ as an electron acceptor. Thereby, *D. vulgaris* can generate both NADH and NADPH via pyruvate → acetyl-CoA to satisfy the energy and biosynthesis requirements. Since the TCA cycle in *D. vulgaris* is mainly for biosynthesis purposes, pyruvate → acetyl-CoA is thus a main step for NADH and NADPH production. The involvement of many different enzymes that function at once for this reaction may improve the flexibility and robustness of *D. vulgaris* metabolism under environmental uncertainty.

Sulfate reduction is an energetically poor process, because reduction of one mole sulfate requires two mole ATP to activate sulfate molecules and four mole NADH to reduce them to H_2S. Thus, sulfate reduction consumes over 80% NADH/NADPH and 90% ATP generated from the lactate → pyruvate → acetate metabolism route (Figure 1). However, an alternative pathway for oxidation of acetyl-CoA to C1 and carbon monoxide where both C1 and carbon monoxide can be further oxidized to CO_2 to generate ATP and NADH has been reported for sulfate reducers (Figure 4). Although most *Desulfovibrio* spp. are thought not to completely oxidize acetyl-CoA (56), key enzymes for such activities are annotated in *D. vulgaris* (Figure 4). These include carbon monoxide dehydrogenase (DVU2098, DVU2099), formate dehydrogenase (e.g.

DVU0587, DVU0588), methylenetetrahydrofolate dehydrogenase / methenyltetrahydrofolate cyclohydrolase (DVU0323). Further, previous reports (53) have shown that a significant amount of carbon monoxide was produced during the growth of *D. vulgaris* in lactate/sulfate medium, consistent with cleavage of acetyl-CoA into C1 and CO (Figure 4). Results from our study support the existence of an acetyl-CoA oxidation pathway (relative flux ~ 5%). The lower measured relative carbon flow to acetate (84%, Figure 1), compared to the expected value (>90%) can be explained by acetyl-CoA oxidation. Additionally, the reactions acetyl-CoA → CO → CO_2 are highly reversible, and thus the C1 of acetyl-CoA exchanges carbon with labeled carbon in CO_2 (removed from pyruvate) via carbon monoxide dehydrogenase (53, 56). The formation of C1-labeled acetyl-CoA may explain why over 20% of leucine's carboxyl group was ^{13}C labeled, even though this carbon is mainly derived from C2 of pyruvate and therefore should not be labeled (Figure 4). Furthermore, since sulfate reduction demands are high for NADH and ATP, acetyl-CoA oxidation may provide an alternate energy producing pathway in *D. vulgaris*. Oxidization of the product [CO] generates hydrogen, which may be used to reduce sulfate and generate ATP (4 mole H_2 generate a net synthesis of 2.7 ATP per mole sulfate reduced); while the product C1 can be oxidized to formate and then CO_2, and those steps also yield ATP and NADH (53, 56).

The TCA cycle is missing two reactions: 1) malate ←→ oxaloacetate, which was not annotated in the *D. vulgaris* genome, and 2) 2-oxoglutarate ←→ succinate. The second reaction has been suggested to be catalyzed by a ferredoxin-dependent enzyme (annotated EC 1.2.7.3) (1) and was found to be active in certain *Desulfobacter*. Flux results supported the genome annotation of two reactions (pyruvate → oxaloacetate (E.C.6.4.1.1) & pyruvate → malate (E.C.1.1.1.4)) that fix CO_2. The $^{13}CO_2$ in the medium was derived mainly from the loss of the

carboxyl group from pyruvate to form acetyl-CoA, whereas unlabeled CO_2 was derived mainly from the gas mix used in the anaerobic chamber. A majority of the aspartate had both carboxyl groups labeled with ^{13}C (M2=0.66). The succinate ^{13}C labeling pattern was similar to that of aspartate (i.e., oxaloacetate), but very different from that of glutamate, which was primarily singly labeled. The flux based on this isotopomer data indicates that succinate was derived from pyruvate and CO_2 through the reductive branch of the TCA cycle, while glutamate was derived from citrate through the oxidative branch of the TCA cycle, i.e., there is no ferredoxin-dependent 2-oxoglutarate synthase (EC 1.2.7.3) activity (2-oxoglutarate + $ferredoxin_{ox}$ + CoA ←→ succinyl-CoA + CO_2 + $ferredoxin_{red}$) (9).

Citrate is a symmetrical molecule, but aconitase is known to be stereospecific for the pro-chiral structure of citrate, providing the stereochemical bias of the reaction (36). The results from the FT-ICR MS analysis of glutamate support a unique carbon transition route (Figure 2) and confirm previous observations that the citrate synthase in *D. vulgaris* has an atypical stereochemical propensity (19, 20). Although the presence of this enzyme has been known for decades, no sequence information is available. Interestingly, an ATP-citrate lyase gene has been annotated in *D. vulgaris* but whether the ATP-citrate lyase is involved in the unusual citrate synthesis requires further study (34).

In SRB, 5,10-Me-THF production controls the mercury methylation pathway, which produces a highly hazardous environmental pollutant (methylated mercury) prone to biomagnification (11, 12). Using ^{14}C labeling, Choi et al. (12) proposed that the 5,10-Me-THF in SRB may originate from two possible sources: serine → glycine + 5,10-Me-THF (5,10-Me-THF from C3 of serine) or from formate via pyruvate formate-lyase: PYR → acetyl-CoA + formate → 5,10-Me-THF (5,10-Me-THF from C1 of pyruvate). Meanwhile, sulfate reducing bacteria can

also convert the C2 of acetyl-CoA to 5,10-Me-THF using the pathway in Figure 4 (49). The labeling pattern of methionine (5 carbon) is similar to that of aspartate (4 carbon), both of which are derived from oxaloacetate. Our results indicate that the methyl of 5,10-Me-THF, which condensed with oxaloacetate to form methionine, was not labeled, demonstrating that 5,10-Me-THF production in *D. vulgaris* is not derived from the formate produced from pyruvate by pyruvate formate-lyase.

The measured biomass contains carbohydrates that are synthesized via glycolysis. However, the flux distribution, based on biomass growth and isotopomer data from histidine and phenylalanine/tyrosine, indicated that no appreciable flow was detectable through the glucose-6-phosphate →→ C5P (ribose-5-phosphate or ribulose-5-phosphate or xylulose-5-phosphate) pathway. This is consistent with the *D. vulgaris* gene annotation, where no candidates were found for two key enzymes (EC1.1.1.49: glucose-6-phosphate dehydrogenase and EC1.1.1.44: phosphogluconate dehydrogenase) in the PP pathway. This is further supported by the lack of any enzyme activity for glucose-6-phosphate dehydrogenase in *D. vulgaris* lysate (i.e., no NADPH is produced via pentose phosphate pathway, unpublished data). Apparently, the incomplete PP pathway is mainly used for biosynthesis of amino acids and nucleic acids. The overall metabolic pathways in *D. vulgaris* are a relatively energetically poor process and appear to be simpler than those in other bacteria, like *E. coli*. From an evolutionary point of view, *D. vulgaris* is thought to present a simple but ancient metabolism developed in the primitive seas (19, 20, 46); understanding its metabolism is potentially important for our understanding the evolution of metabolic pathways in early life.

Conclusion

We used non-radioactive tracer experiments and isotopomer analysis to examine the key annotated metabolic pathways in *D. vulgaris* as well as to quantify carbon flux through these pathways. Both GC-MS and FT-ICR MS techniques were used to obtain complete isotopomer information for the metabolites for subsequent isotopomer analysis. Data from this study confirmed several aspects of *D. vulgaris* metabolism, such as an incomplete pentose phosphate pathway, a branched and incomplete TCA cycle, the presence of an R-citrate synthase and acetyl-CoA oxidation route. This study demonstrates FT-ICR MS to be a potential tool for flux analysis with several advantages over conventional methods. Compared to GC-MS, samples do not need to be derivatized and therefore the data can be used without correction for the natural isotopomer effect from the derivatized group. Compared to NMR spectroscopy, FT-ICR MS is a much more sensitive method with a very low detection limit (order of nmol). FT-ICR MS enables the localization of labeled carbon at locations not accessible via GC-MS or ^{13}C NMR. ESI FT-ICR MS did not require the separation of metabolites by GC or HPLC, and thus is a high throughput method for measuring the isotopomers compared to other methods which require separation prior to detection.

The isotopomer distribution data was essential to confirm the result that key central pathways in *D. vulgaris* are incomplete. However, due to the low flux (<5%) in the PP pathway and TCA cycle, the precise flux values and their reversibility through these pathways could not be ascertained using the isotopomer data. In this study, estimation of the fluxes towards central pathways, biomass synthesis and other metabolites (acetate, pyruvate and succinate) relied primarily on direct measurement of the production rates of these metabolites.

Abbreviations

[CO], bound carbon monoxide; C1, 5,10-Me-THF; C5P, ribose-5-phosphate or ribulose-5-phosphate or xylulose-5-phosphate; CIT, citrate; E4P, erythrose-4-phosphate; F6P, fructose-6-phosphate; FUM, fumarate; G6P, glucose-6- phosphate; ICT, isocitrate; MAL, malate; OAA, oxaloacetate; OXO, 2-oxoglutarate; PEP, phospho*enol*pyruvate; PGA, 3-phosphoglycerate;PYR, pyruvate; S7P, sedoheptulose-7-phosphate; SUC, succinate; T3P, 3- phosphate-glyceraldehyde; All amino acids use their standard abbreviations.

Acknowledgements

We thank Professor Judy Wall (University of Missouri, Columbia) for helpful discussions on *D. vulgaris* pathways. Dr. Steve Van Dien (Genomatica Company) provided the isotopomer correction spreadsheet. Adam Meadows, Kenneth Kauffman, Jeannie Chu (University of California, Berkeley), Rick Huang (Lawrence Berkeley National Laboratory) and Gary Kruppa (Bruker Daltonics CA, USA) helped with experiments and isotopomer modeling. This work is part of the Virtual Institute for Microbial Stress and Survival (http://vimss.lbl.gov) supported by the U.S. Department of Energy, Office of Science, Office of Biological and Environmental Research, Genomics:GTL Program through contract DE-AC02-05CH11231 between the Lawrence Berkeley National Laboratory and the US Department of Energy.

Reference

1. **Alm, E. J., K. H. Huang, M. N. Price, R. P. Koche, K. Keller, I. L. Dubchak, and A. P. Arkin.** 2005. The MicrobesOnline Web site for comparative genomics. Genome Res **15:**1015-22.
2. **Arauzo-Bravo, M. J., and K. Shimizu.** 2003. An improved method for statistical analysis of metabolic flux analysis using isotopomer mapping matrices with analytical expressions. Journal of Biotechnology **105:**117-133.
3. **Badziong, W., B. Ditter, and R. K. Thauer.** 1979. Acetate and carbon dioxide assimilation by *Desulfovibrio vulgaris* (Marburg), growing on hydrogen and sulfate as sole energy source. Archives of Microbiology **123:**301-305.
4. **Beranova, S., J. Cai, and C. Wesdemiotis.** 1995. Unimolecular Chemistry of Protonated Glycine and Its Neutralized Form in the Gas Phase. Journal of the American Chemical Society **117:**9492-9501.
5. **Blanch, H. W., and D. S. Clark.** 1997. Biochemical Engineering. Marcel Dekker Inc., New York.
6. **Bond, D. R., T. Mester, C. L. Nesbo, A. V. Izquierdo-Lopez, F. L. Collart, and D. R. Lovley.** 2005. Characterization of citrate synthase from *Geobacter sulfurreducens* and evidence for a family of citrate synthases similar to those of eukaryotes throughout the Geobacteraceae. Appl Environ Microbiol **71:**3858-65.
7. **Boopathy, R.** 2002. Methanogenesis from furfural by defined mixed cultures. Current Microbiology **44:**406-410.
8. **Brown, S. C., G. Kruppa, and J. L. Dasseux.** 2005. Metabolomics application of FT-ICR mass spectrometry. Mass Spectrometry Reviews **24:**223-231.
9. **Buchanan, B. B.** 1969. Role of ferredoxin in the synthesis of α-ketobutyrate from propionyl coenzyme A and carbon dioxide by enzymes from photosynthetic and nonphotosynthetic bacteria. The Journal of Biological Chemistry **244:**4218-4223.
10. **Chhabra, S. R., Q. He, K. H. Huang, S. P. Gaucher, E. J. Alm, Z. He, M. Z. Hadi, T. C. Hazen, J. D. Wall, J. Zhou, A. P. Arkin, and A. K. Singh.** 2006. Global Analysis of Heat Shock Response in *Desulfovibrio vulgaris Hildenborough*. J Bacteriol **188:**1817-28.
11. **Choi, S. C., and R. Bartha.** 1994. Environmental factors affecting mercury methylation in estuarine sediments. Bull Environ Contam Toxicol **53:**805-12.
12. **Choi, S. C., T. Chase, and R. Bartha.** 1994. Metabolic Pathways Leading to Mercury Methylation in *Desulfovibrio desulfuricans* LS. Appl Environ Microbiol **60:**4072-4077.
13. **Cooney, M. J., E. Roschi, I. W. Marison, C. Comninellis, and U. V. Stockar.** 1996. Physiologic studies with the sulfate-reducing bacterium *Desulfovibrio desulfuricans*: Evaluation for use in a biofuel cell. Enzyme and Microbial Technology **18:**358-365.
14. **Cornish-Bowden, A., and M. L. Cardenas.** 2000. From genome to cellular phenotype--a role for metabolic flux analysis? Nat Biotechnol **18:**267-8.
15. **Daniels, L., R. S. Hanson, and et al.** 1994. Chemical Analysis, p. 512-554. *In* P. Gerhardt, R. Murray, W. Wood, and N. Krieff (ed.), Method for General and Molecular Bacteriology. American Society of Microbiology, Washington DC.
16. **Fischer, E., and U. Sauer.** 2005. Large-scale *in vivo* flux analysis shows rigidity and suboptimal performance of *Bacillus subtilis* metabolism. Nature Genetics **37:**636-640.

17. **Fischer, E., and U. Sauer.** 2003. Metabolic flux profiling of *Escherichia coli* mutants in central carbon metabolism using GC-MS. Euro. J. Biochem **270:**880-891.
18. **Gevertz, D., A. J. Telang, G. Voordouw, and G. E. Jenneman.** 2000. Isolation and characterization of strains CVO and FWKO B, two novel nitrate-reducing, sulfide-oxidizing bacteria isolated from oil field brine. Appl Environ Microbiol **66:**2491-501.
19. **Gottschalk, G.** 1968. The stereospecificity of the citrate synthase in sulfate-reducing and photosynthetic bacteria. European J. Biochem, **5:**346-351.
20. **Gottschalk, G., and H. A. Barker.** 1967. Presence and stereospecificity of citrate synthase in anaerobic bacteria. Biochemistry **6:**1027-1034.
21. **Hadas, O., and R. Pinkas.** 1995. Sulfate reduction processes in sediments at different sites in lake kinneret, israel. Microbial Ecology **30:**55-66.
22. **Harrison, A. G., and Y. P. Tu.** 1998. Ion chemistry of protonated aspartic acid derivatives. Journal of Mass Spectrometry **33**.
23. **Harrison, G. A.** 2001. Ion chemistry of protonated glutamic acid derivatives. International Journal of Mass Spectrometry **210/211:**361-370.
24. **He, Q., K. H. Huang, Z. He, E. J. Alm, M. W. Fields, T. C. Hazen, A. P. Arkin, J. D. Wall, and J. Zhou.** 2006. Energetic consequences of nitrite stress in *Desulfovibrio vulgaris Hildenborough*, inferred from global transcriptional analysis. Applied and Environmental Microbiology **72:**4370-4381.
25. **Heidelberg, J. F., R. Seshadri, S. A. Haveman, C. L. Hemme, I. T. Paulsen, J. F. Kolonay, J. A. Eisen, N. Ward, B. Methe, L. M. Brinkac, S. C. Daugherty, R. T. Deboy, R. J. Dodson, A. S. Durkin, R. Madupu, W. C. Nelson, S. A. Sullivan, D. Fouts, D. H. Haft, J. Selengut, J. D. Peterson, T. M. Davidsen, N. Zafar, L. Zhou, D. Radune, G. Dimitrov, M. Hance, K. Tran, H. Khouri, J. Gill, T. R. Utterback, T. V. Feldblyum, J. D. Wall, G. Voordouw, and C. M. Fraser.** 2004. The genome sequence of the anaerobic, sulfate-reducing bacterium *Desulfovibrio vulgaris Hildenborough*. Nat Biotechnol **22:**554-9.
26. **Hellerstein, M. K., and R. A. Neese.** 1999. Mass isotopomer distribution analysis at eight years: theoretical, analytic, and experimental considerations. American Journal of Physiology-Endocrinology and Metabolism **276:**E1146-E1170.
27. **Humphries, A. C., and L. E. Macaskie.** 2002. Reduction of Cr(VI) by *Desulfovibrio vulgaris* and *Microbacterium sp*. Biotechnology Letters **24:**1261-1267.
28. **Humphries, A. C., K. P. Nott, L. D. Hall, and L. E. Macaskie.** 2004. Continuous removal of Cr(VI) from aqueous solution catalysed by palladised biomass of Desulfovibrio vulgaris. Biotechnol Lett **26:**1529-32.
29. **Laskin, J., and J. H. Futrell.** 2003. Collisional activation of peptide ions in FT-ICR mass spectrometry. Mass Spectrometry Reviews **22:**158-181.
30. **Lewis, A. J., and J. D. Miller.** 1977. The tricarboxylic and acid pathway in Desulfovibrio. Can J Microbiology **23:**916-921.
31. **Marshal, J.** 2004. Production of secondary metabolites from acetyl Co-A precursors in bacterial and fungal hosts. PhD thesis. University of California, Berkeley.
32. **Marshall, A. G., C. L. Hendrickson, and G. S. Jackson.** 1998. Fourier Transform Ion Cyclotron Resonance Mass Spectrometry: A Primer. Mass Spectrometry Reviews **17:**1-35.
33. **McLafferty, F. W., Turecek F.** 1993. Interpretation of Mass Spectra. Fourth Edition. University Science Books, Sausalito, CA.

34. **Moller, D., R. Schauder, G. Fuchs, and R. K. Thauer.** 1987. Acetate oxidation to CO_2 via a citric acid cycle involving an ATP-citrate lyase: a mechanism for the synthesis of ATP via substrate level phosphorylation in *Desulfobacter postgatei* growing on acetate and sulfate. Archives of Microbiology **148:**202-207.
35. **Mukhopadhyay, A., Z. He, E. J. Alm, A. P. Arkin, E. E. Baidoo, S. C. Borglin, W. Chen, T. C. Hazen, Q. He, H. Y. Holman, K. Huang, R. Huang, D. C. Joyner, N. Katz, M. Keller, P. Oeller, A. Redding, J. Sun, J. Wall, J. Wei, Z. Yang, H. C. Yen, J. Zhou, and J. D. Keasling.** 2006. Salt Stress in *Desulfovibrio vulgaris Hildenborough*: an Integrated Genomics Approach. J Bacteriol **188:**4068-78.
36. **Nelson, D. L., and M. M. Cox.** 2000. Lehninger Principles of Biochemistry. Worth Publishers, New York.
37. **Nemati, M., G. E. Jenneman, and G. Voordouw.** 2001. Mechanistic study of microbial control of hydrogen sulfide production in oil reservoirs. Biotechnol Bioeng **74:**424-34.
38. **Noguera, D. R., G. A. Brusseau, B. E. Rittmann, and D. A. Stahl.** 1998. A Unified Model Describing the Role of Hydrogen in the Growth of *Desulfovibrio vulgaris* under Different Environmental Conditions. Biotechnology and Bioengineering **59:**732-746.
39. **Noguera, D. R., G. A. Brusseau, B. E. Rittmann, and D. A. Stahl.** 1998. Unified model describing the role of hydrogen in the growth of *Desulfovibrio vulgaris* under different environmental conditions. Biotechnology and Bioengineering **59.:**732-746.
40. **Ouattara, A. S., and V. A. Jacq.** 1992. Characterization of sulfate-reducing bacteria isolated from senegal rice fields. Fems Microbiology Ecology **101.:**217-228.
41. **Sauer, U., D. R. Lasko, J. Fiaux, M. Hochuli, R. Glaser, T. Szyperski, K. Wuthrich, and J. E. Bailey.** 1999. Metabolic flux ratio analysis of genetic and environmental modulations of *Escherichia coli* central carbon metabolism. Journal of Bacteriology **181:**6679-6688.
42. **Schmidt, K., J. Nielsen, and J. Villadsen.** 1997. Modeling isotopomer distributions in metabolic networks using isotopomer mapping matrices. Biotechnology and Bioengineering **55:**831-840.
43. **Schmidt, K., J. Nielsen, and J. Villadsen.** 1999. Quantitative analysis of metabolic fluxes in *Escherichia coli*, using two-dimensional NMR spectroscopy and complete isotopomer models. Journal of Biotechnology **71:**175-190.
44. **Stelling, J., U. Sauer, Z. Szallasi, F. Doyle, and J. Doyle.** 2004. Robustness of cellular functions. Cell **118:**675-685.
45. **Stephanopoulos, G. N., A. A. Aristidou, and J. Nielsen.** 1998. Metabolic Engineering Principles and Methodologies. Academic Press, San Diego.
46. **Stern, J. R., C. S. Hegre, and G. Bambers.** 1966. Glutamate biosynthesis in anaerobic bacteria. II. stereospecificity of aconitase and citrate synthetase of *Clostridium kluyveri*. Biochemistry **5:**1119.
47. **Szyperski, T.** 1998. 13C-NMR, MS and metabolic flux balancing in biotechnology research. Quarterly Reviews of Biophysics **31:**41-88.
48. **Teece, M. A., M. L. Fogel, M. E. Dollhopf, and K. H. Nealson.** 1999. Iostopic fraction associated with biosynthesis of fatty acids by a marine bacterium under oxic and anoxic conditions. Organic Geochemistry **30:**1571-1579.
49. **Thauer, R. K.** 1988. Citric-acid cycle, 50 years on modifications and an alternative pathway in anaerobic bacteria. European J. Biochem, **176:**497-508.

50. **Traore, A. S., M. L. Fardeau, C. E. Hatchikian, J. L. Gall, and J. P. Belaich.** 1983. Energetics of Growth of a Defined Mixed Culture of *Desulfovibrio vulgaris* and Methanosarcina barkeri: Interspecies Hydrogen Transfer in Batch and Continuous Cultures. Applied and Environmental Microbiology **46:**1152-1156.
51. **Traore, A. S., C. E. Hatchikian, J. P. Belaich, and J. L. Gall.** 1981. Microcalorimetric Studies of the Growth of Sulfate-Reducing Bacteria: Energetics of *Desulfovibrio vulgaris* Growth. Journal of Bacteriology **145:**191-199.
52. **Tu, Y. P., Harrison, A. G.** 1998. The b1 ion derived from methionine is a stable species. Rapid Communication in Mass Spectrometry **12:**849-851.
53. **Voordouw, G.** 2002. Carbon monoxide cycling by *Desulfovibrio vulgaris Hildenborough*. Journal of Bacteriology **184:**5903-5911.
54. **Voordouw, G., S. M. Armstrong, M. F. Reimer, B. Fouts, A. J. Telang, Y. Shen, and D. Gevertz.** 1996. Characterization of 16S rRNA genes from oil field microbial communities indicates the presence of a variety of sulfate-reducing, fermentative, and sulfide-oxidizing bacteria. Appl Environ Microbiol **62:**1623-9.
55. **Wahl, S. A., M. Dauner, and W. Wiechert.** 2004. New tools for mass isotopomer data evaluation in ^{13}C flux analysis: mass isotope correction, data consistency checking, and precursor relationships. Biotechnology and Bioengineering **85:**259-68.
56. **White, D.** 1995. The Physiology and Biochemistry of Prokaryotes. Oxford University Press, New York.
57. **Wiechert, W., and A. A. de Graaf.** 1997. Bidirectional reaction steps in metabolic networks I. Modeling and simulation of carbon isotope labeling experiments. Biotechnology and Bioengineering **55:**101-117.
58. **Zhao, J., and K. Shimizu.** 2003. Metabolic flux analysis of Escherichia coli K12 grown on 13C-labeled acetate and glucose using GC-MS and powerful flux calculation method. Journal of Biotechnology **101:**101-117.

Figure Captions

Figure 1. Flux distribution in *D. vulgaris*. Fluxes were estimated from measurements taken at mid-log phase (30~40 hrs) and normalized by the average lactate uptake rate in log phase (13.8±1.8 mmol hr^{-1} gdw^{-1}). The solid arrows indicate reactions that are active. A dotted arrow indicates that the reaction has zero flux based on enzyme and isotopomer data. An 'x' indicates the absence of an annotated gene for the step. The data in brackets are the exchange coefficients of reactions that are significantly reversible based on isotopomer model analysis. Based on the flux distribution, partial oxidation of 1 mole lactate produces ~2.0 mol NADH/NADPH and ~0.9 mol ATP; sulfate reduction ($Y_{SO4/Lac}$=0.4) (mol/mol) consumes 1.6 mol NADH, and uses 0.8 mol ATP per mole lactate to activate sulfate groups.

Figure 2. Transition of carbons in the synthesis of citrate from lactate reflects the prochiral nature of citrate in the TCA cycle (a symmetrical molecule that reacts asymmetrically). Oxaloacetate is the precursor of aspartic acid. 2-Oxoglutarate is the precursor of glutamate. FT-ICR MS spectrum of glutamic acid confirms that the C5 carbon (#) originated from the C4 carbon of oxaloacetate, and the C1 carbon (^) of glutamic acid originated from the C1 carbon of acetyl-CoA.

Figure 3. FT-ICR MS to locate the ^{13}C carbon position in glutamate. **(a)** SORI-CID (MS^2) of $[^{13}C\text{-Glu+H}]^+$ generated by ESI. The fragmentation includes no loss (m/z 149), loss of H_2O (m/z 131), loss of H_2O and CO (α) (m/z 103), and loss of 2 H_2O and CO (α) (m/z 85). The data in parenthesis are the measurement errors expressed in ppm. **(b)** SORI-CID (MS^3) of m/z 85

generated in the ICR cell. Ion (m/z 56) indicates that the remaining carbon bone was not labeled after loss of the second carboxyl group.

Figure 4. Acetyl-CoA oxidization and leucine biosynthesis. The C1 and C2 carbons of leucine originated from the C1 and C2 of acetyl-CoA. Acetyl-CoA can be reversibly oxidized via an alternative pathway. C1 is 5,10-Me-THF. [CO] is bound carbon monoxide. Annotated enzymes involved in acetyl-CoA oxidization: reaction 1 (methylenetetrahydrofolate dehydrogenase, methenyltetrahydrofolate cyclohydrolase); reaction 2 (formate dehydrogenase); reaction 3 (carbon monoxide dehydrogenase).

Figure 1

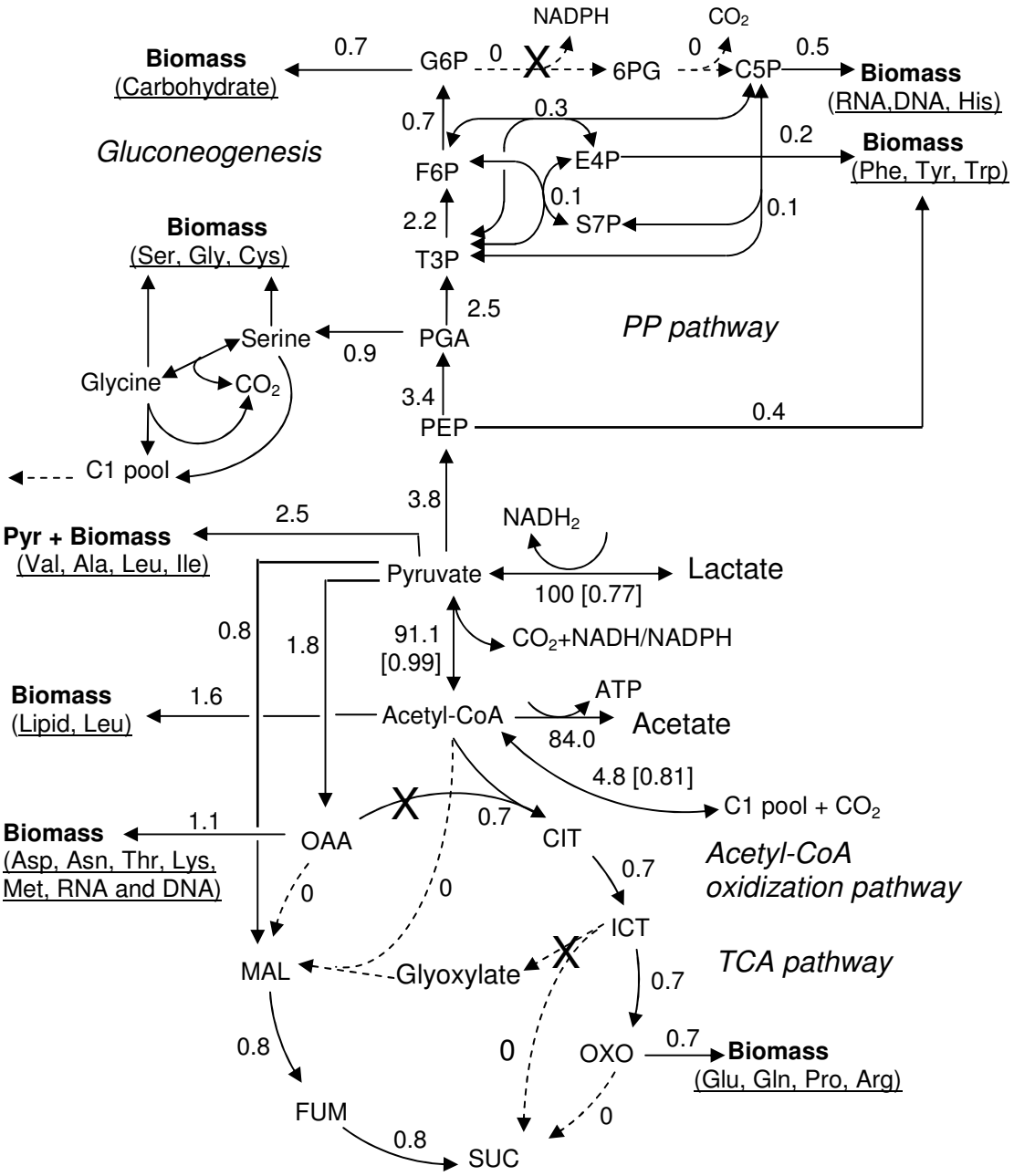
NADPH
CO2
Biomass
(Carbohydrate)
0.7
G6P
0
6PG
0
C5P
0.5
Biomass
(RNA,DNA, His)
0.7
0.3
Gluconeogenesis
0.2
Biomass
(Phe, Tyr, Trp)
F6P
E4P
0.1
2.2
S7P
0.1
Biomass
(Ser, Gly, Cys)
T3P
2.5
PP pathway
Serine
PGA
0.9
Glycine
CO2
3.4
0.4
PEP
C1 pool
3.8
2.5
NADH2
Pyr + Biomass
(Val, Ala, Leu, Ile)
Pyruvate
Lactate
100 [0.77]
0.8
1.8
91.1
[0.99]
CO2+NADH/NADPH
Biomass
(Lipid, Leu)
1.6
Acetyl-CoA
ATP
Acetate
84.0
4.8 [0.81]
C1 pool + CO2
1.1
0.7
Biomass
(Asp, Asn, Thr, Lys,
Met, RNA and DNA)
OAA
CIT
Acetyl-CoA
oxidization pathway
0
0
0.7
ICT
MAL
Glyoxylate
TCA pathway
0.7
0.8
0
OXO
0.7
Biomass
(Glu, Gln, Pro, Arg)
FUM
0
0.8
SUC

Figure 2

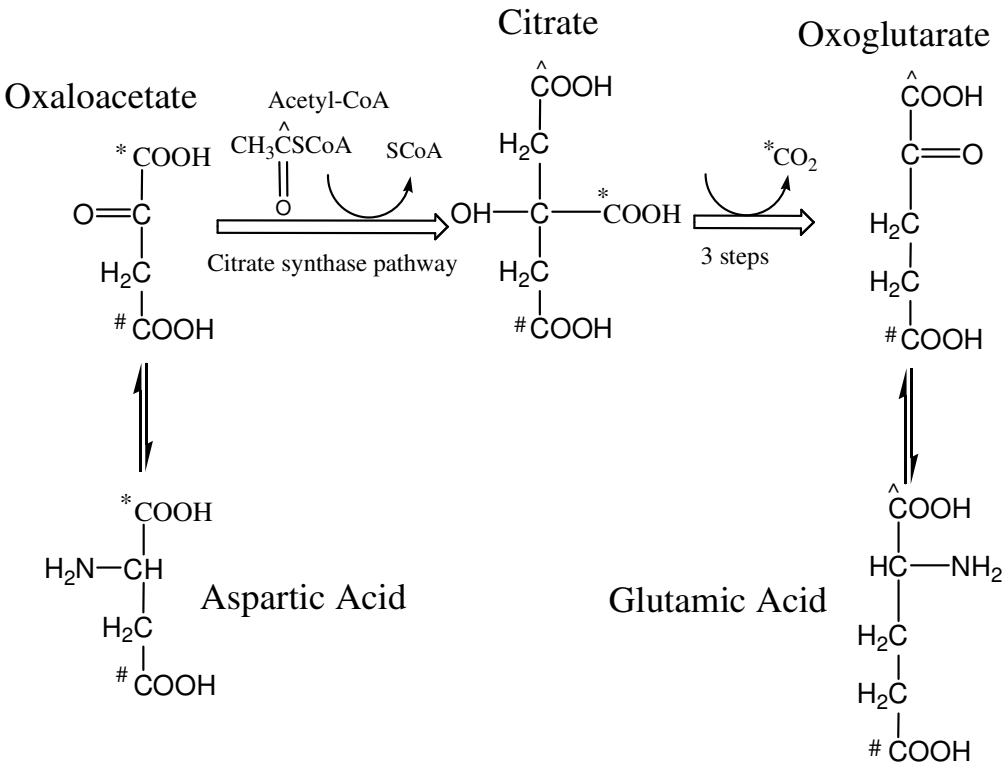
Oxaloacetate
Acetyl-CoA
Citrate
Oxoglutarate
SCoA
Citrate synthase pathway
3 steps
Aspartic Acid
Glutamic Acid

Figure 3

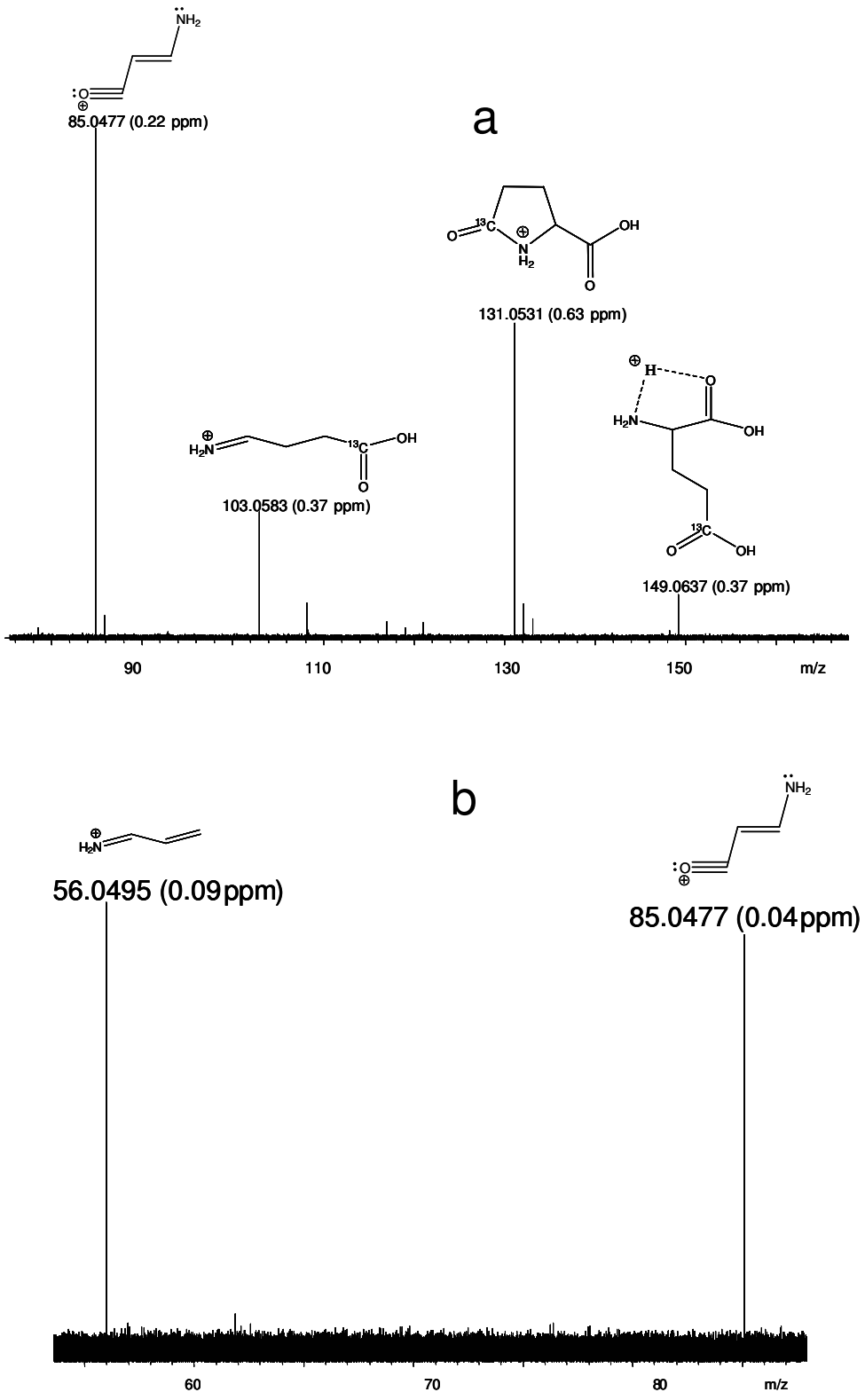
a
85.0477 (0.22 ppm)
131.0531 (0.63 ppm)
103.0583 (0.37 ppm)
149.0637 (0.37 ppm)
90
110
130
150
m/z
b
56.0495 (0.09ppm)
85.0477 (0.04ppm)
60
70
80
m/z

Figure 4

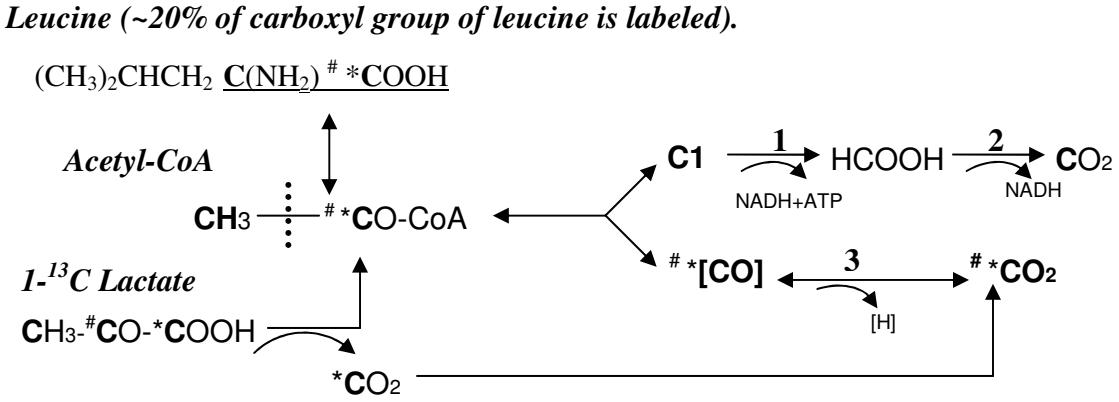
Leucine (~20% of carboxyl group of leucine is labeled).
(CH3)2CHCH2 C(NH2) # *COOH
Acetyl-CoA
CH3 # *CO-CoA
1-13C Lactate
CH3-#CO-*COOH
*CO2
C1
1
HCOOH
2
CO2
NADH+ATP
NADH
*[CO]
3
*CO2
[H]

Tables

Table 1. Kinetic parameters for growth of *Desulfovibrio vulgaris* Hildenborough in LS4D lactate medium.

Report kinetics	**$Y_{X/C}$ (g/mole)**	**$Y_{SO4/Lac}$ (mol/mol)**	**$t_{1/2}$ (hr*)**	**μ_{max} (hr^{-1})**	**K_s (mM)**	**Product (mol/mol lactate)**
This study	6.1 ± 0.8	0.40 ± 0.05	8.2 ±2.0	0.10 ±0.01	27 ±2	acetate: 0.84± 0.03 alcohol: <0.002 pyruvate:~0.02 succinate:~0.01
1.Ref. (51) 2.Ref.(38)	5.3~6.8[1, 2]	0.4~0.57[2]	2.7 ~4.3[1]	0.22 ~0.27[1,2]	29[2]	acetate: 0.97[1] ethanol: ~0.02[1] H_2: up to 0.5

Table 2. Measured and model predicted (in parenthesis) fragment mass distributions for ^{13}C-labeled metabolites from *D. vulgaris* hydrolysates or supernatant [1].

Amino acids (Precursors)	Fragment	M0	M1	M2	M3	C13 enriched position
Glycine (PEP)	No loss	0.17 (0.15)	0.82 (0.82)	0.01 (0.02)		carboxyl group
Serine (PEP)	No loss	0.17 (0.15)	0.81 (0.82)	0.02 (0.02)		carboxyl group
	Loss of COOH	0.98 (0.97)	0.02 (0.03)	0 (0)		
Alanine (Pyruvate)	No loss	0.17 (0.16)	0.81 (0.82)	0.02 (0.03)		carboxyl group
	Loss of COOH	0.97 (0.96)	0.03 (0.04)	0.0 (0)		
Leucine[2] (Pyruvate and acetyl CoA)	No loss	0.75 (0.89)	0.23 (0.10)	0.02 (0.01)		carboxyl group
	Loss of COOH	0.95 (0.94)	0.03 (0.02)	0.01 (0.01)		
Glutamate (OXO)	No loss	0.21 (0.20)	0.73 (0.74)	0.06 (0.06)		C5 carboxyl group
	Loss of COOH	0.22 (0.21)	0.77 (0.76)	0.01 (0.02)		
Asparate (OAA)	No loss	0.04 (0.03)	0.29 (0.30)	0.66 (0.65)	0.01 (0.02)	C1 or C4 carboxyl group
	Loss of COOH	0.20 (0.21)	0.79 (0.76)	0.01 (0.02)		
Methionine (OAA)	No loss	0.04 (0.03)	0.27 (0.30)	0.65 (0.65)	0.02 (0.02)	carboxyl group
	Loss of COOH	0.20 (0.21)	0.75 (0.76)	0.03 (0.02)	0.02 (0.0)	
Histidine (C5P)	No loss	0.16 (0.12)	0.62 (0.64)	0.11 (0.12)	0.11 (0.12)	The carboxyl group is NOT enriched.
	Loss of COOH	0.17 (0.12)	0.62 (0.64)	0.11 (0.12)	0.12 (0.12)	
Phenylalanine (PEP+E4P)	No loss	0.03 (0.0)	0.12 (0.06)	0.35 (0.31)	0.50 (0.57)	The carboxyl group
	Loss of COOH	0.04 (0.02)	0.32 (0.25)	0.60 (0.65)	0.03 (0.05)	
Lactate	No loss	0.08 (0.10)	0.91 (0.89)	0.02 (0.01)		carboxyl group
	Loss of COOH	0.96 (0.96)	0.03 (0.04)	0.01 (0.0)		
Succinate	No loss	0.07 (0.03)	0.26 (0.30)	0.67 (0.65)	0 (0.01)	C1 or / and C5 carboxyl group
Predicted CO_2		(0.22)	(0.78)			

1. ^{13}C-Labeled biomass was sampled in the middle log phase in the LS4D medium (n=4). The complete data for isotopomer distribution and standard deviation of all amino acids are listed as supplemental materials Table S-4.

2. FT-ICR MS cannot distinguish the mass distributions between leucine and isoleucine, because both molecules have same mass molecular weight. GC-MS cannot measure the ion fragment (M-57)+ (no loss) accurately because of the overlay of mass peaks by (f302)+ (fragment with only α and β carbon of leucine).